Multi-relation octomap based Heuristic ICP for air/surface robots cooperation

Conference Paper · December 2015

DOI: 10.1109/ROBIO.2015.7418987

CITATION
1

READS
17

4 authors:

Peng Yin
Carnegie Mellon University
14 PUBLICATIONS **28** CITATIONS
SEE PROFILE

Yu Qing He
Shenyang Institute of Automation, Chinese Academy of Sciences, Shenyang, China
162 PUBLICATIONS **568** CITATIONS
SEE PROFILE

Feng Gu
Chinese Academy of Sciences
41 PUBLICATIONS **108** CITATIONS
SEE PROFILE

Jianda Han
Chinese Academy of Sciences
316 PUBLICATIONS **2,289** CITATIONS
SEE PROFILE

Proceedings of the 2015
IEEE Conference on Robotics and Biomimetics
Zhuhai, China, December 6-9, 2015

Multi-relation Octomap Based Heuristic ICP for Air/Surface robots Cooperation*

Peng Yin, Yuqing He, Feng Gu and Jianda Han

Abstract— **In this paper, we focus on the problem of fast and accurate featureless registration of outdoor large scale 3D point-clouds which possess great differences in the aspects of both resolution and view of point. There are two main methods generally used to solve this problem: feature based algorithm and point based one. However, feature based method can only be used in very special environments with clear geometric structure, while traditional point based method can only obtain a relative coarse estimation and is sensitive to initial alignment. Thus, in this paper, a registration algorithm, called Octree Based Multiresolution Heuristic ICP, is proposed.**

Without relying on the good initial registration and marked features, hybrid-ICP combines different ICP algorithms, and improve the alignments using finer levels of representation.

In our outdoor riverside environments experiments, our method outperform the classical point based registration algorithm with an accuracy of 7 times better than classical Generalized-ICP and a speedup 1.6 times.

I. INTRODUCTION

Multi-type robots cooperation navigation system shows much more advantages than traditional robot navigation system, especially in field environment. Generally, the single robot system or single-type robots system lack the property of navigating the full range of the scene. The views of robots such as unmanned ground vehicle (UGV) or unmanned surface vehicle (USV), could be blocked by local obstacles, and they also suffer from vibration of rough road or water waves, severe noisy measurements, as well as complex terrains. To efficiently navigate the environment, views of different type robots can be combined to make a global alignment, there for both relative position and local view can be learned.

Registration point-clouds with different resolution (RPDR) has been there for real applications in many area, such as medical and robotics. Barratt [1] combine CT scan and freehand 3D ultrasound (US) to make the alignment for the femur and pelvis model. Nicola[2] use an air-ground cooperation method to registration two different types of point-cloud to help the UGV locate in the airborne LiDAR map and make the global path planning at the same time. By using RPDR, the local robots can efficient find their location in the global map and get higher resolution view around them. But to efficiently align point-clouds with different resolutions and high terrain noise is not an easy task. We take three different point-cloud data sets from a water side, respectively, they are from an UGV, an USV and an unmanned aerial vehicle (UAV). As shown in [2], the real time registration algorithm of RPDR problem involve three steps: 1) Find correspondence points in each points; 2) Calculate the average square root of distance, if the distance is small than certain value, then output the transform result, else go to step 3; 3) Estimate the transform matrix based on distance; 4) Convert the point-cloud by transform matrix, and go back to step 1. The mainly difference between various alignment method is based on the step 1. There mainly have two major scheme: the feature-based method and point-based method[3].

In applications, the feature-based scheme always considers some certain kind of feature descriptors. In reference[4], the Harris corner detector[5] and the SUSAN corner detector[6] were suggested to register the range data of lasers. But since few edges or corner features can be found in nature environment, these algorithms are difficult to be implemented. Chua [7] introduced point signature, a special kind of local point feature descriptor, to search for correspondences. The main drawback of this algorithm is the procedure to compute the point signature, which needs too much time. In reference [2] and[8910], spin-image[11] is used to realize model registration. Spin-image is a rigid transformation invariant local feature descriptor and is of great accuracy and robustness. He[12] has pointed out that spin-image based registration method is often time consuming because it need to calculate the spin images of each point in both global map and local map. Compared with the feature based method, the point-based schemes gain much more attentions, and the Iterative Closest Point (ICP) algorithm [131415] is one of the most referred to. ICP algorithm, originally applied to scan-matching in the early 90s, has been extensively researched over the past decade and a half. In essential, ICP is a local registration method and requires a good initial alignment, i.e., bad initial estimation may deteriorate the registration results greatly. Generalized-ICP (GICP) [16] is a robust ICP variant, it converts the point-to-point comparison to plane-to-plane, so even with badly-estimation it could still achieve a good alignment. But this method is time consuming, because it need to calculate the covariance matrix of selected points to find the correspondence.

The applications of above-mentioned algorithm in field experiment show that feature-based methods often require clear geometric features and high resolution data sets which are overwhelming for field robots, and the performance of point-based methods usually depend on initial alignment. Without a relative good initial registration, point-based methods usually sinks into a local optimal solution. To compensate for the non-

*Research supported by the State Key Program of National Natural Science of China (Grant No. 61473282, 61203340).

Peng Yin is with the State Key Laboratory of Robotics, Shenyang Institute of Automation, Chinese Academy of Sciences, Shenyang 110016, University of Chinese Academy of Sciences, Beijing 100049, China. yinpeng@sia.cn.

Yuqing He, Feng GU and Jianda Han are with the State Key Laboratory of Robotics, Shenyang Institute of Automation, Chinese Academy of Sciences, Shenyang 110016, China.

978-1-4673-9675-2/15/$31.00 © 2015 IEEE

uniform point densities, we proposed a novel Multi-Resolution Based Hybrid ICP Registration method. First after the initial filtering, two type point-cloud models are transforming into a same plane by using a Ransac algorithm. Then a point-to-point based standard-ICP method transforms the local scan model into an initial registration by making the alignment from low resolution to relatively high resolution. Finally a Generalized-ICP is taken to refine the registration result. Through this process certain thresholds are taken to decide which ICP method to use and a jump method improve the robustness to avoid local optimal.

II. Motivation and Method

Because our work is based on the traditional ICP method, in this section, we first introduce Standard-ICP, Generalized-ICP and Multi-Resolution ICP.

A. Standard-ICP

The classical ICP method [7] and its variations have been well studied over the past two decades, and till now there are more than 400 papers around this issue. Standard ICP is an efficient method to deal with rigid registration, generally, rigid registration is a procedure to determine a rigid transformation between two point sets so that correspondent points can be matched. Consider tow point sets $P=\{\mathrm{p}_i\}_{i=1}^{N_n}$ and $X=\{\mathrm{x}_j\}_{j=1}^{N_m}$ in R^m (also referred to the data shape and model shape, respectively), we wish to minimize a cost function over all Translate T of P relative to X:

$$\min_{R,t,j\in\{1,2,\ldots,\mathrm{N}_m\}}\Big(\sum_{i}^{N_n}\|(\mathrm{R}\mathrm{p}_i+t)-x_j\|_2^2\Big)$$
$$\mathrm{s.t.}\,\mathrm{R}^T R=I_m,\det(\mathrm{R})=1 \qquad (1.1)$$

where $R\in R^{m\times m}$ is a rotation matrix, and t is a translation vector. The rigid registration can be achieve by tow iterative steps.

Firstly, the $(\mathrm{k}-1)^{th}$ rigid transformation $(\mathrm{R}_{k-1},\mathrm{t}_{k-1})$ is used to find correspondence $\{\mathrm{p}_i,\mathrm{x}_{c_k(\mathrm{i})}\}$ between two point sets P and X, which is shown as below:

$$c_k(\mathrm{i})=\underset{j\in\{1,2,\ldots,\mathrm{N}_m\}}{\arg\min}\,(\|(\mathrm{R}_{k-1}\mathrm{p}_i+\mathrm{t}_{k-1})-x_j\|_2^2),\mathrm{i}=1,2,\ldots,\mathrm{N}_n \quad (1.2)$$

Secondly, the new rigid translation $(\mathrm{R}^*,\mathrm{t}^*)$, between two point sets $\{\mathrm{R}_{k-1}\mathrm{p}_i+\mathrm{t}_{k-1}\}_{i=1}^{N_n}$ and $\{\mathrm{x}_{c_k(\mathrm{t})}\}_{i=1}^{N_m}$ is computed based on $c_k(\mathrm{i})$:

$$(\mathrm{R}^*,\mathrm{t}^*)=\underset{R^tR=\mathrm{I}_m,\det(\mathrm{R})=1}{\operatorname{argmin}}\Big(\sum_{i=1}^{N_n}\|\mathrm{R}(\mathrm{R}_{k-1}\mathrm{p}_i+\mathrm{t}_{k-1})+\mathrm{t}-x_{c_k(\mathrm{i})}\|_2^2\Big) \qquad (1.3)$$

Update R_k and t_k in k^{th}:

$$R_k=R^*R_{k-1},t_k=R^*t_{k-1}+t^* \qquad (1.4)$$

While the standard ICP is a local convergent method, for a successful registration process, the initial rigid translation is important to guarantee the best matching between two point sets.

B. Generalized-ICP

The standard ICP algorithm is a Point-To-Point approach, which means that it tries to align all matched point exactly be minimizing their Euclidean distance. This doesn't take into account that an exact matching is usually not feasible because the different sampling of the two point clouds leads to pairs without perfect equivalence. Figure 1 illustrates two point clouds, both being different samplings of the same scene. The Standard-ICP alignment result shows that the red data could should be shifted to the left for a perfect alignment, but this would increase three of the pairs' distances while reducing only two, which would deteriorate the result in terms of the strict Point-To-Point metric.

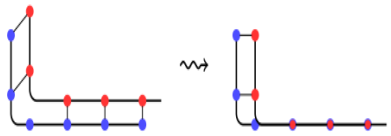

Figure 1 The Point-To-Point matching of Standard-ICP can lead to a poor alignment.

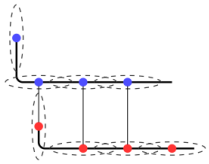

Figure 2 The confidence ellipses show how the probabilistic Plane-To-Plane model of the Generalized-ICP works.

To overcome this issue, some variants of ICP take advantage of the surface normal information. While Point-To-Plane variants consider just the surface normal from the model point cloud, Plane-To-Plane variants use the normal from both model and data point cloud. The Generalized-ICP (GICP) algorithm in [16] belongs to the second category. It use a probabilistic model to modify the error function by assigning a covariance matrix to each point. This is based on the assumption that every measured point results from an actually existing point and the sampling can be modeled by a multivariate normal distribution. The outcome of the derivation in [16] is the new error function:

$$T^*=\underset{T}{\arg\min}\sum_i d_i^{(\mathrm{T})^T}(\mathrm{C}_i^A+\mathrm{T}\mathrm{C}_i^B\mathrm{T}^T)^{-1}d_i^{(\mathrm{T})} \qquad (1.5)$$

where $d_i^{(\mathrm{T})}=a_i-Tb_i$ with covariance matrices C_i^A and C_i^B. An appropriate selection of C_i^A and C_i^B can reproduce the error function of the Standard-ICP or a Point-To-Plane variant [16]. In general, the covariance matrix must be rotated for every point depending on its surface normal. The covariance matrices are visualized as confidence ellipses: the position of a point is known with high confidence along the normal, but the exact location in the plane is unsure.

The effect is that corresponding points are not directly dragged onto another, but the underlying surface represented by the covariance matrices are aligned. The covariance matrices are aligned. The covariance matrices are computed so that they express the expected uncertainty along the local surface normal at the point. The Generalized-ICP algorithm is

more robust than the standard ICP method. Because of computing the covariance matrices and Eigen decompositions of the empirical covariance, Generalized-ICP cost more time than standard-ICP.

C. Multi Resolution ICP

The work of Jost[17] et al. shows that there are two methods to accelerate the Standard ICP method: the k-D tree structure and the multiresolution shame. From $O(\mathrm{N}_p\mathrm{N}_x)$ .originally, it becomes $O(\mathrm{N}_p\log\mathrm{N}_x)$ with a tree search. Assume we reduce both the data model and shape model by a factor N , the speed up gain is:

$$\begin{aligned} Gain_{speed} &= O(\mathrm{N}_p\log\mathrm{N}_x)/O(\frac{\mathrm{N}_p}{N}\log\frac{\mathrm{N}_x}{N}) \\ &= \mathrm{O}(\mathrm{N}\frac{\log N_x}{\log N_x-\log N}) > \mathrm{O}(\mathrm{N}) \end{aligned} \tag{1.6}$$

If we examine the k-D tree case, the value of $\log N_x/(\log N_x-\log N)$ is typically situated between 1 and 2, and so the $Gain_{speed}$ on average is more than N .

Now, say m to be the number of iterations needed for a constant resolution, n_i the number of iterations at resolution step i for the same registration in a k steps multiresolution shame as shown in Figure 3. And C_i is the cost of registration at step i . The total cost of an algorithm with constant resolution is $C_{tot,mono}=m\cdot C_1$ and $C_{tot,mono}=n_1C_1+n_2C_2+\ldots+n_kC_k$ of the multiresolution shame, the total gain is:

$$\begin{aligned} G_{total} &= \frac{C_{tot,mono}}{C_{tot,multi}} = \frac{mC_1}{n_1C_1+n_2C_2+\ldots+n_kC_k} \\ &= \frac{m}{n_1+\frac{n_2}{N}+\ldots+\frac{n_k}{N^{k-1}}} \end{aligned} \tag{1.7}$$

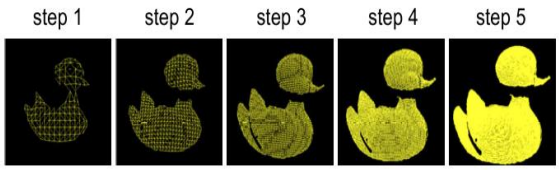

Figure 3 The multiresolution step

Jost [18] has proved that G_{total} is increment, taking into account how the iteration times changes with different resolution. Because the ICP method highly depend on the initial alignment, the coarse to fine registration method can find a good estimate at first which will help to reduce the iterative time at high resolution.

III. Registration

The model and scene in RPDR problem have significant differences in scale, rotation, translation and point density. And point-clouds in field environment usually have different levels of noise and outliers. To apply the registration process, a preprocessing step which include proper step filters is needed for both model and scene.

The main part of our algorithm is a Hybrid-ICP loop. This method takes advantages of both standard-ICP and Generalized-ICP. Firstly, a tow-step standard-ICP is used to find a rough alignment from coarse to fine resolution maps where the maps are generated from an octree structure. Based on the alignment Index, it can be indicate the efficiency of previous registration. If the index is high enough, which means continue the 2-step-ICP can still make a better alignment. Or if index is not high enough as we expected, a deep resolution map is given to make a newer alignment by using standard-ICP or Generalized-ICP method. At the worst case, Alignment index is getting worse, which means the registration hit a local optimal, a lift action is taken to avoid this situation.

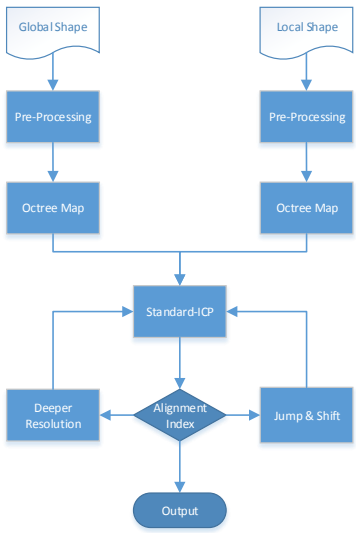

Figure 4 Flowchart of registration process: The main loop is combined with standard-ICP and General-ICP method. Firstly, the 2-step standard-ICP is used to find the rough alignment from crude to fine resolution maps. If score1 is high enough, we continue the first step, or make a deep resolution action or scene lift action based on how worse the score1. Secondly, a newer alignment is obtained by a standard-ICP or Generalized-ICP, and output the alignment score2. When score2 couldn't improve any longer, the final alignment is achieved.

A. Octree-based fusion map

Octree is a tree-type data structure where each internal node has exactly eight children. Octree is often used to partition a 3D space by recursively subdividing it into eight octants. The point sets fusion is achieved by using an occupancy grid mapping method[19]. The probability $P(\mathrm{n}\,|\,\mathrm{s}_{1:t})$ of a leaf node n means the probability of this node being occupied given the sensor measurements $s_{1:t}$ which are from the starting point to current state,

$$P(\mathrm{n}\,|\,\mathrm{s}_{1:t}) = [1+\frac{1-P(\mathrm{n}\,|\,\mathrm{s}_t)}{P(\mathrm{n}\,|\,\mathrm{s}_t)}\frac{1-P(\mathrm{n}\,|\,\mathrm{s}_{t-1})}{P(\mathrm{n}\,|\,\mathrm{s}_{t-1})}\frac{P(\mathrm{n})}{1-P(\mathrm{n})}]^{-1} \tag{1.8}$$

where $P(\mathrm{n})$ means the prior probability of node n being occupied. This update formula depends on the current measurement z_t , a prior probability P_n , and the previous estimate $P(\mathrm{n}\,|\,\mathrm{s}_{1:t})$. The term $P(\mathrm{n}\,|\,\mathrm{s}_t)$ denotes the

probability of voxel n to be occupied given the measurement z_t . Equation 8 can be rewritten as:

$$\frac{1-P(\mathrm{n}\mid \mathrm{s}_{1:t})}{P(\mathrm{n}\mid \mathrm{s}_{1:t})}=\frac{1-P(\mathrm{n}\mid \mathrm{s}_{t})}{P(\mathrm{n}\mid \mathrm{s}_{t})}\cdot\frac{1-P(\mathrm{n}\mid \mathrm{s}_{1:t-1})}{P(\mathrm{n}\mid \mathrm{s}_{1:t-1})}\frac{1-P(\mathrm{n})}{P(\mathrm{n})} \tag{1.9}$$

Normally, the common assumption of a uniform prior probability leads to $P(\mathrm{n})=0.5$ and by using the log-odds notation, Equation.9 can be written as

$$L(\mathrm{n}\mid \mathrm{z}_{1:t})=\mathrm{L}(\mathrm{n}\mid \mathrm{z}_{1:t})+\mathrm{L}(\mathrm{n}\mid \mathrm{z}_{t}) \tag{1.10}$$

$$L(\mathrm{n})=\log(\frac{P(\mathrm{n})}{1-P(\mathrm{n})}) \tag{1.11}$$

When measurements are integrated into the map structure, probabilistic updates are performed only for the leaf nodes in the octree. Since an octree is hierarchical data structure, we can make use of the inner nodes in the tree to enable multiresolution shames. Several policies can be used to update the tree, according to our application, the maximum occupancy method is used here.

$$L_j(\mathrm{n})=\max_i L_{j+1}(\mathrm{n}_i),\mathrm{i}=1,...,8 \tag{1.12}$$

where $L_j(\mathrm{n})$ is the n^{th} node in the j level resolution map, and n_i is the eight sub node in $j+1$ level resolution map.

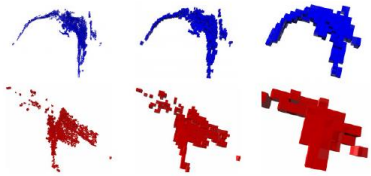

Figure 5 Multi-resolution Grid Map

Based on the hierarchical octree map, both the global shape and the local shape can achieve different schemes at multi-resolution level. In our application, the global shape are obtained with a MAV, and the point cloud are processed offline. While the local shapes are achieved by a UAV and a UGV, and they are analyzed by combining the offline global shape in real time, which we will extended in the Section 4.

B. *Heuristic-ICP*

Based on the multiresolution maps obtained by the octree structure, the Standard ICP method is to be used in the coarse-to-fine registration algorithm. The Basic Heuristic-ICP method is given in Algorithm 1. Given global shape, local shape and the initial resolution grid level (the real distance between to point), the Standard-ICP method can achieve the coarse-to-fine multiresolution registration. As shown in line 3 and line4, if the alignment score is bigger than a threshold θ_1 , then the resolution extended to the higher level. But generally, the Standard-ICP couldn't guarantee to achieve a global optimal. And if the initial alignment error is too big, the Standard-ICP could stocked into a local optimal. As we have stated in section in 2.B, the Generalized-ICP could be used here.

An upward action is taken to assist such situation. In line 6, if the Score is below 0 (the registration has hit a local optimal), we restore the previous alignment and move upward for two Resolution grid unit according to the current level. The Point-To-Point based Standard-ICP couldn't get it out of the local optimal. As we have seen in Section 2.B, Plane-To-Plane based Generalized-ICP could efficiently find the better alignment. Both the global map and the local map update the $i-1$ level resolution map. At the same time, the local map move upward for a certain distance and make the alignment by using the Generalized-ICP.

Another important key step is to efficiently calculate the jump orientation. We estimate the direction by considering the point sets $Q=\{\mathrm{q}^1,\mathrm{q}^2,...,\mathrm{q}^{Nc}\}$ in local map that have found correspondence in the global map. For each point in Q , find its k nearest points in point set Q , and the covariance matrix of point q^j could be given as:

$$Cov=\frac{1}{k}\sum_{i=1}^{k}(q_i^j-\bar{q}^j)\cdot(q_i^j-\bar{q}^j)^T \tag{1.13}$$

$$\bar{q}^j=\frac{1}{k}\sum_{i=1}^{k}q_i^j \tag{1.14}$$

We can calculate the eigenvalue of the covariance matrix by:

$$Cov\cdot v_t^j=\lambda_t^j\cdot v_t^j,\mathrm{t}\in\{0,1,2\} \tag{1.15}$$

where λ_t^j is the covariance matrix's t^{th} eigenvalue, and v_t^j is the relevant t^{th} feature vector. Assume the eigenvalues are numbered according to their value:

$$\lambda_0^j\geq\lambda_1^j\geq\lambda_2^j \tag{1.16}$$

According to sod work, the vector v_2^j of the minimum eigenvalue λ_2^j is the normal vector of point q^j . We estimate the average normal vector by:

$$v=\frac{1}{N_c}\sum_{j=1}^{N_c}v_2^j \tag{1.17}$$

Usually the jump distance is depend on the current resolution level, and here we set it at 10 times resolution grid according to our experiment test.

IV. Experiment and Results

A. *Experiment Setup*

To verify the proposed algorithm, experiments are conducted on an Unmanned Surface Vehicle (USV) and an Unmanned Aerial Vehicle (UAV). The vehicle is equipped with navigation system for pose estimation and LiDAR for environment perception. The navigation system measures the vehicle pose by an IMU (inertial measurement unit) and a GPS. The pose is outputted at 100 Hz frequency. The velocity error of the navigation system is 0.028 m/s, the heading error is 0.1° , the roll and pitch error is 0.05° . The LiDAR system is a HDL-32E from Velodyne. The 3D LiDAR is set to spin at 10 Hz. About 700,000 points are generated per second by each 3D LiDAR. The error of 3-D LiDAR is 20 mm at 25 m. Measurements from the navigation system and LiDAR are

collected and processed to map the surrounding environment by a laptop (model: Think-pad x220, configuration: Intel i5-2410M 4 core @ 2.30 GHz CPU and 8 GB RAM) from Lenovo. The software is programmed by C++ in the ROS (Robot Operating System) framework [16].

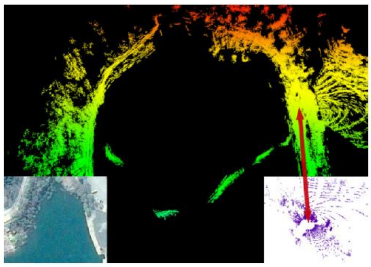

Figure 6 Large Scene Point Cloud Model

The environment is at a riverside, and the point-clouds of model and scene are generated from the LiDAR system on the USV, but they are from two data sets which were recorded at different time and with diverse resolutions. The model point-cloud is obtained by using the GICP method to align 100 different point-clouds $\{Cloud_1, Cloud_2 \cdots Cloud_{100}\}$, which were taken from both the water surface and the ground. Each point-cloud contains about 40,000 points, and the near point-clouds ($Cloud_i$ and $Cloud_{i+1}$) have small transfer error. After voxel grid compressing, the model point-cloud have 500,000 points, with a scope of $200m \times 300m$ and the resolution of 1m. The point-cloud of scene is generated from the same LiDAR system but at a different time, and it only contain 40,000 points, with a scope of $40m \times 30m$ and the resolution of 2m. The detail information is given in TABLE 1.

TABLE I
DATA SETS

Data set	Points	Scope (in x y plane)	Resolution
Global map	8,900,000	$200m \times 300m$	1m
Local scan	$40,000 \pm 10,000$	$40m \times 30m$	2m

TABLE II
TEST SETS

Data set	Max $Trans_e$	Max Rot_x	Max Rot_y	Max Rot_z
Low error	5m	10°	10°	10°
Middle error	15m	20°	20°	20°
High error	30m	30°	30°	40°

To test our algorithm with others, we generated many different scenes which are obtained from initial perfect matched point-clouds by using a random transformation. Here the initial aligned point is matched with the model point-cloud by using many different tools under the human operation which is accurate but time consuming. According the transformation distance and rotation on each axis, the scenes could be categorized to three kind data sets. The detail information of the three data sets are given in TABLE 2.

To measure the accuracy of different method, here we calculate the mean square error between the original perfect alimented local scan with the data set that is calculated out by Standard-ICP, Generalized-ICP or our method:

$$\begin{aligned} \Delta x_i &= x_{original[i]} - x_{align[i]} \\ \Delta y_i &= y_{original[i]} - y_{align[i]} \\ \Delta z_i &= z_{original[i]} - z_{align[i]} \\ Error &= \sqrt{\frac{\sum(\Delta x_i^2 + \Delta y_i^2 + \Delta z_i^2)}{N_p}}, i = 1,.., \mathrm{N}_p \end{aligned} \tag{1.18}$$

where N_p is the number of points in local scan point-cloud , $x_{original[i]}$, $\mathrm{y}_{original[i]}$, $\mathrm{z}_{original[i]}$ are the i^{th} original point's coordinates along the xyz axis, and $x_{align[i]}$, $\mathrm{y}_{align[i]}$, $\mathrm{z}_{align[i]}$ are the i^{th} alimented point's coordinates by calculated.

B. Application result and analysis

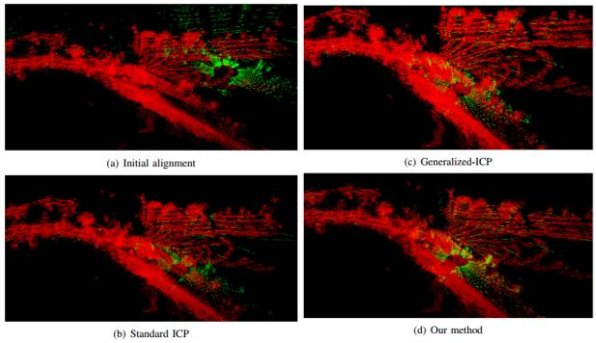

Figure 7 Registration result: (a) initial alignment, (b) Standard ICP method, (c) Generalized ICP method, (d) our method.

We test the Standard-ICP, Generalized-ICP and our method in the three test data sets, and one example is picked up here to the result of three algorithm in Fig.7. The red point-cloud represents the model (global map), and the green point-cloud represents the scene (local scan). This scene belongs to the middle error data sets, where the translation is (15, 14, 15) and rotation $(15^\circ, -15^\circ, 20^\circ)$ to its matched point-cloud.

The alignment of standard ICP method is given in Fig.7b, the transfer error is 8.43m, and this process is finished in 51.2ms. In Fig.7c, Compare to the Standard ICP, Generalized-ICP method gives a better alignment result and it is very robust to the translation and rotation error. In this case, the transfer error of Generalized-ICP is 2.12m and the computation time is 3680ms which is more than 70 times to the standard-ICP. In our method, by mixture the advantage of this two algorithm with the multi-resolution method, both the accuracy and computation time is improved. In this case, our method takes 1578ms and achieve a better accuracy at 0.34m, which cost a half time of Generalized-ICP but gets a 6 times better result. Another advantage of our method is the automatically adjust property which benefits from the auto lift-up action. Even the first alignment is fall into a local minimal, the point-cloud of the scene can be lift upwards for d_z and continue to find a better alignment. Especially in the high error transfer case, while both standard-ICP and Generalized-ICP fail to find the

match, our algorithm can still find an accurate alignment with this method.

TABLE III
TRANSFER ERROR

Accuracy	Low error	Middle error	High error	Average
Our method	0.56m	1.19m	5.32m	2.35m
Standard-ICP	6.35m	21.71m	42.93m	23.67m
Generalized-ICP	0.83m	9.49m	39.83m	16.72m

TABLE IV
RUNNING TIME

Time consuming	Low error	Middle error	High error	Average
Our method	2248ms	2161ms	2933ms	2447ms
Standard-ICP	52ms	53ms	53ms	53ms
Generalized-ICP	3317ms	4656ms	3919ms	3995ms

We give 12 test results in each category. In the low-resolution test, our method could not achieve a better result at some samples, but in the middle and high resolution test our method could achieve a significant good result than others. Especially in the high-resolution test, both the standard-ICP and Generalized-ICP failed to find a match as in the Fig.7c. The average transfer error and running time are calculate in each categories and in all sample as shown in TABLE 3 and TABLE 4. In the running time of high error case, we ignore the samples where the Generalized-ICP failed (the running time is within 300ms). Our method can achieve an accuracy 7 times better than Generalized-ICP and 10 times than standard-ICP, and a speed 1.6 times better than Generalized-ICP.

V. CONCLUSIONS

This paper proposed a multi-resolution based Hybrid-ICP Registration method to efficiently find the alignment transformation without an initial estimation. Instead of finding local descriptor, a multi-resolution method is used to efficiently give a relatively good initial estimate. We combine the standard-ICP method and the robust Generalized-ICP method to balance the speed and accurate. A choice mechanism is taken to decide how to switch different ICP methods. An auto lift-up action is taken to avoid our search algorithm hit a better optimal. In our experiment, our method achieve an accuracy 7 times better than Generalized-ICP and 10 times than standard-ICP, and a speed 1.6 times better than Generalized-ICP.

REFERENCES

1 Barratt. DC; Chan. CSK; Edwards. PJ; Penney, Penney. Graeme P, "Instantiation and registration of statistical shape models of the femur and pelvis using 3D ultrasound imaging," MEDICAL IMAGE ANALYSIS, vol. 12, pp. 358-374

2 N. Vandapel, R. R. Donamukkala, and M. Hebert, "Unmanned Ground Vehicle Navigation Using Aerial Ladar Data," Int. J. Rob. Res., vol. 25, pp. 31–51, 2006.

3 R. B. Rusu and S. Cousins, "3D is here: point cloud library," IEEE Int. Conf. Robot. Autom., 2011.

4 A. Downs, R. Madhavan, and T. Hong,"Registration of range data from unmanned aerial and ground vehicles," in Applied Imagery Pattern Recognition Workshop, 2003. Proceedings. 32nd, 2003, pp. 45-50.

5 K. Derpanis, "The harris corner detector," York Univ., pp. 2–3, 2004.

6 S. Smith and J. Brady, "SUSAN—a new approach to low level image processing," Int. J. Comput. Vis., vol. 23, no. 1, pp. 45–78, 1997.

7 C. S. Chua and R. Jarvis, "Point signatures: A new representation for 3d object recognition," International Journal of Computer Vision, vol. 25, pp. 63-85, 1997.

8 He Yuqing and Mei Yuangang, An efficient registration algorithm based on spin image for LiDAR 3D point cloud models, Neurocomputing, 2015, Vol. 151, Part 1, 354-363.

9 H. Quynh Dinh and S. Kropac, "Multi-resolution spin-images," in Proceedings of the IEEE Computer Society Conference on Computer Vision and Pattern Recognition, 2006, vol. 1, pp. 863–870.

10 J. Assfalg, M. Bertini, A. D. Bimbo, and P. Pala, "Content-Based Retrieval of 3-D Objects Using Spin Image Signatures," IEEE Trans. Multimed., vol. 9, no. 3, 2007.

11 A. E. Johnson, Using Spin-Images for Efficient Object Recognition in Cluttered 3-D Scenes, no. July, 1998.

12 He Yuqing and Mei Yuangang, An efficient registration algorithm based on spin image for LiDAR 3D point cloud models, Neurocomputing,

13 P. Besl and N. McKay, "A Method for Registration of 3-D Shapes," IEEE Transactions on Pattern Analysis and Machine Intelligence, vol. 14. pp. 239–256, 1992.

14 Y. Chen, G. Medioni. "Object Modeling by Registration of Multiple Range Images," Proc. of the 1992 IEEE Intl. Conf. on Robotics and Automation, pp. 2724-2729, 1991.

15 Z. Zhang, "Iterative point matching for registration of free form curves and surfaces," Int. J. Comput. Vis., vol. 12, no. 1994, pp. 119–152, 1994.

16 A. Segal, D. Haehnel, and S. Thrun, "Generalized-ICP," Robot. Sci. Syst., 2009.

17 T. Jost and H. Hugli, "A multi-resolution ICP with heuristic closest point search for fast and robust 3D registration of range images," Fourth Int. Conf. 3-D Digit. Imaging Model. 2003. 3DIM 2003. Proceedings, no. 3dim, pp. 0–6, 2003.

18 T. Jost and H. Hugli, "A multi-resolution scheme ICP algorithm for fast shape registration," Proceedings. First Int. Symp. 3D Data Process. Vis. Transm., 2002.

19 Moravec H, Elfes A (1985) High resolution maps from wide angle sonar. In: Proc. Of the IEEE Int. Conf. on Robotics & Automation (ICRA), St. Louis, MO, USA, pp 116-121